American Mineralogist, Volume 84, pages 1588–1594, 1999

In situ X-ray diffraction study of enstatite up to 12 GPa and 1473 K and equations of state

TORU SHINMEI,[1,*] NAOTAKA TOMIOKA,[1] KIYOSHI FUJINO,[1] KOJI KURODA,[2] AND TETSUO IRIFUNE[2]

[1]Division of Earth and Planetary Sciences, Graduate School of Science, Hokkaido University, N10 W8, Kita-ku, Sapporo 060-0810, Japan
[2]Department of Earth Sciences, Faculty of Science, Ehime University, 2-5 Bunkyo-cho, Matsuyama, 790-8577, Japan

ABSTRACT

Crystal structures and phase transitions of enstatite ($MgSiO_3$) were studied by in situ X-ray diffraction experiments using synchrotron radiation and a multi-anvil high-pressure apparatus at pressures to 12 GPa and temperatures to 1473 K. Low clinoenstatite with space group $P2_1/c$ transforms to high-pressure $C2/c$ clinoenstatite at high pressures and high temperatures, accompanied by a volume reduction of about 2.5%. The β angle of this high-pressure $C2/c$ phase ranges from 101.4° to 101.7°, shows almost no variation with pressure and temperature, and is about 8° smaller than that of the high-temperature $C2/c$ phase previously reported. This confirms the suggestion (Hugh-Jones et al. 1994) that these two clinoenstatite phases differ at high pressures and high temperatures. The pressure-volume-temperature data for $P2_1/c$ and high pressure $C2/c$ clinoenstatite were fit to room-temperature third-order Birch-Murnahan equations of state (EOS) using the parameters: volume of V_0 = 415.4 (5) Å^3, isothermal bulk modulus of K_0 = 108.5 (6.4) GPa, and its pressure derivative of K_0' = 4.5 (1.3) for the $P2_1/c$ phase, and V_0 = 405.1 (1.7) Å^3, K_0 = 106.4 (17.4) GPa, and K_0' = 5.4 (2.7) for the $C2/c$ phase. These values are at ambient conditions. For the $C2/c$ phase, we determined the high-temperature EOS, expressed as $P = 3/2\ K_T\ [(V_T/V)^{7/3}–(V_T/V)^{5/3}]\{1–3/4\ (4–K_T')[(V_T/V)^{2/3}–1]\}$, where $K_T = K_0 + (\partial K_T/\partial T)_P\ (T–300)$, $K_T' = K_0'$, $V_T = V_0\ [\exp(\int_{300}^{T} \alpha(T)\mathrm{d}T)]$, where thermal expansivity $\alpha(T)$ is $a_0 + a_1\ T$. The parameters are V_0 = 405.0 (2.6) Å^3, K_0 = 106.9 (25.9) GPa, K_0' = 5.3 (3.9), a_0 = 2.01 (44) × 10^{-5} K^{-1}, a_1 = 2.10 (1.1) × 10^{-8} K^{-2}, and $(\partial K_T/\partial T)_P$ = –0.021 (10) GPa/K. Although the K_0 values are nearly the same with those of previous studies for both the $P2_1/c$ and $C2/c$ phases, the K_0' values are slightly smaller.

INTRODUCTION

Enstatite is one of the major constituent minerals in the Earth's crust and the upper mantle. Enstatite of pure $MgSiO_3$ composition is reported to have five polymorphs, orthoenstatite with space group *Pbca* (Morimoto and Koto 1969), protoenstatite with *Pbcn* (Atlas 1952; Brown and Smith 1963; Smyth 1971; Chen and Presnall 1975; Yang and Ghose 1995), low clinoenstatite with $P2_1/c$ (Morimoto et al. 1960), high-temperature (high-*T*) clinoenstatite with $C2/c$ (Smith 1969; Sadanaga and Okamura 1971; Gasparik 1990; Shimobayashi and Kitamura 1991, 1993; Iishi and Kitayama 1995), and high-pressure (high-*P*) clinoenstatite with $C2/c$ (Pacalo and Gasparik 1990; Angel et al. 1992). Protoenstatite is reported to be a stable phase above ~1273 K at atmospheric pressure, but below that temperature, orthoenstatite is considered to be stable (Brown and Smith 1963; Boyd and Schairer 1964; Smyth 1974). The stability field of low clinoenstatite was studied by Sclar et al. (1964) using belt type apparatus, and by Boyd and England (1965) using piston cylinder apparatus. These authors reported that low clinoenstatite is stable at temperatures below ~900 K. In contrast, deformation experiments of orthoenstatite showed that shear stress affects the orthoenstatite–low clinoenstatite inversion boundary, suggesting the possibility that low clinoenstatite has no stability field under hydrostatic conditions (Riecker and Rooney 1967; Munoz 1968; Coe 1970; Raleigh and Kirby 1971). The subsequent study by Grover (1972) through hydrothermal runs using $MgCl_2 \cdot H_2O$ flux at pressures up to 4 kbar, reports that low clinoenstatite is stable below 839 K at atmospheric pressure. However, the precise trajectory of the phase boundary between orthoenstatite and low clinoenstatite in *P-T* space is unclear.

Hydrostatic high-pressure experiments using a multi-anvil cell (MAC) high-pressure apparatus have shown that clinoenstatite has a stability field under high pressure and high temperature (Yamamoto and Akimoto 1977; Pacalo and Gasparik 1990; Kanzaki 1991). Subsequent high-pressure in situ single-crystal X-ray diffraction experiments at room temperature using a diamond anvil cell (DAC) have shown that $P2_1/c$ low clinoenstatite transforms between 6.98 GPa and 7.93 GPa upon compression to non-quenchable high-*P* clinoenstatite with space group $C2/c$ (Angel et al. 1992). This high-*P* $C2/c$ phase is also reported at pressures above 5 GPa and at room temperature by Raman spectra (Chopelas and Boehler 1992) and the single crystal compression study of ferrosilite ($FeSiO_3$) using a DAC (Hugh-Jones et al. 1994). However, there had

*Present address: Institute for Study of the Earth's Interior, Okayama University, Yamada 827, Misasa, Tottori-ken, 682-0193, Japan. E-mail: shinmei@misasa.okayama-u.ac.jp

been no in situ X-ray diffraction data of the $C2/c$ phase of enstatite at high pressure and high temperature to obtain accurate equations of state.

This paper presents in situ X-ray diffraction experiments of enstatite at pressures to 12 GPa and temperatures to 1473 K using a MAC high-pressure apparatus and synchrotron radiation. From measured pressure-volume-temperature data, the equations of state for $P2_1/c$ and high-P $C2/c$ clinoenstatite were derived using a third-order Birch-Murnahan equation of state.

Experimental methods and analytic procedure

In situ X-ray diffraction experiments

In situ X-ray diffraction experiments at high pressures and high temperatures were performed using the MAX 80 system (Shimomura et al. 1985; Yagi 1988), a MAC high-pressure apparatus combined with synchrotron radiation, at the National Laboratory for High Energy Physics (KEK), Tsukuba, Japan. The sample assembly and experimental technique are essentially the same as that of Irifune et al. (1998). The hybrid anvil system, consisting of four tungsten carbide (WC) anvils and four advanced diamond composite (ADC) anvils, was used for the second-stage MA 8-type anvils (Irifune et al. 1992). The incident synchrotron X-ray beam was directed onto the sample through the anvil gap via a 50 μm horizontal slit and 300 μm vertical slit. The diffracted beam was collected via a 50 μm horizontal slit and 500 μm vertical slit. A collimator that has a 50 μm horizontal slit was also used to collect the information from a limited region of the sample. X-ray diffraction experiments were made by the energy dispersive method at a fixed 2θ angle of 4.0° using a white X-ray spectrum. The precise 2θ scale was calibrated using the (111), (200), and (220) reflections of gold at ambient conditions. Synthetic pure $MgSiO_3$ low clinoenstatite with space group $P2_1/c$ was used as a starting material. The powdered sample, mixed with Au powder for the pressure standard material, was enclosed in a capsule made of cemented amorphous boron. TiC twin-sheet heaters were used, and temperatures were measured by a W5%Re-W26%Re thermocouple. X-ray diffraction patterns were obtained from the sample and the Au pressure standard material close to the thermocouple junction, and temperature uncertainty was thus estimated to be less than ~50 K. No correction for the pressure effects on the electromotive force (EMF) was applied. Semi-sintered magnesia, mixed with a trace of cobalt, was used for the pressure transmitting medium. Pressures were calculated by the refined unit-cell volumes of Au and measured temperatures, using the third-order Birch-Murnahan equation of state for Au (Anderson et al. 1989) as follows:

$$P\,(V,\,T\,)–P\,(V_0,\,300) = 3/2\;K_0\;[(V_0/V\,)^{7/3}–(V_0/V\,)^{5/3}]\{1–3/4\,(4–K_0')[(V_0/V)^{2/3}–1]\} + [\,7.14\times10^{-3} + (\partial K_T/\partial T\,)_V \ln\,(V_0/V\,)](T–300), \quad (1)$$

with values of K_0 = 166.65 GPa, K_0' = 5.5, V_0 = 67.85 Å^3, and $(\partial K_T/\partial T\,)_V = –11.5\times10^{-3}$ GPa/K. The unit-cell volumes of Au were refined by the least-squares technique using the (111), (200), and (220) reflections. Differences of the pressure calculated from the different peaks of Au in a same run are less than 0.4 GPa and no systematic errors have been observed among them.

The P-T paths in the experiments are shown in Figure 1. Each symbol on all paths in Figure 1 indicates the point at which X-ray diffraction data were taken in about 100–1000 seconds. The unit-cell parameters of the observed phases were refined by the least-squares technique using 10 to 23 reflections.

Equation-of-state calculation

First, the pressure-volume data at room temperature for the $P2_1/c$ and high-P $C2/c$ phases were fit to a third-order Birch-Murnahan equation of state, which is given by:

$$P = 3/2\;K_0\,[(V_0/V)^{7/3}–(V_0/V)^{5/3}]\{1–3/4\,(4–K_0')[(V_0/V)^{2/3}–1]\}. \quad (2)$$

Second, the entire pressure-volume-temperature data set for the high-P $C2/c$ phase was fit to the high temperature form of a third-order Birch-Murnahan (HTBM) equation of state (Saxena and Zhang 1990). The HTBM equation of state used here has the same form as the Equation 2, but K_0, K_0', and V_0 are replaced by K_T, K_T', and V_T which are the values at temperature to incorporate temperature effects. K_T and V_T are given by:

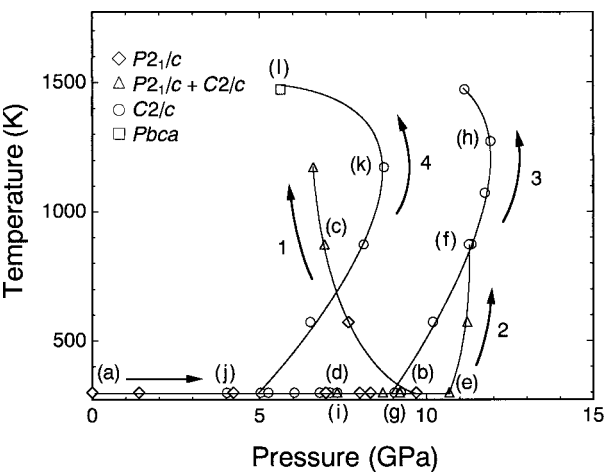

Figure 1. Temperature-pressure paths of the in situ X-ray diffraction experiments. Symbols at the points along the P-T paths 1 to 4 indicate the identified phases. Diamonds = $P2_1/c$ low clinoenstatite; circles = high-P $C2/c$ clinoenstatite; triangles = $P2_1/c$ + high-P $C2/c$; squares = *Pbca* orthoenstatite. The sample was first compressed to 9.7 GPa at room temperature (point b). Then, temperature was increased to 1173 K at a constant press load, which resulted in the decrease of sample pressure because the pyrophyllite gaskets and pressure transmitting medium flowed (path 1). The sample was then quenched to room temperature, where sample pressure became 7.3 GPa (d). The sample was compressed again up to 10.7 GPa at room temperature (e), and then temperature was increased to 873 K (f), following path 2. In this heating process, sample pressure was slightly increased probably because the strain in the cell had already been relaxed. After the sample was quenched (g), temperature was increased again up to 1473 K, following path 3. When the sample was quenched, pressure dropped to 7.3 GPa (i), and then the sample was decompressed down to 4.0 GPa at room temperature (j). After the sample was compressed again to 5.0 GPa, temperature was increased to 1473 K(l), following path 4, and then the sample was quenched and slowly decompressed to atmospheric pressure.

$$K_T = K_0 + (\partial K_T/\partial T)_P\,(T\text{–}300) \quad (3)$$

$$V_T = V_0\left[\exp\left(\int_{300}^{T}\alpha(T)\mathrm{d}T\right)\right]. \quad (4)$$

In this study, we used the following expression for the thermal expansion coefficient:

$$\alpha(T) = a_0 + a_1\,T, \quad (5)$$

where a_0 and a_1 are constants. In the present HTBM equation of state calculation, $K_T' = K_0'$ was assumed and all six fitting parameters were simultaneously refined using a Marquardt method.

RESULTS AND DISCUSSION

In situ X-ray diffraction patterns and lattice parameters

The obtained X-ray diffraction patterns at the points a–l on the *P-T* paths in Figure 1 are illustrated in Figure 2. In the initial compression up to 9.7 GPa at room temperature (b), the width of diffraction peaks became broad and close peaks overlapped with each other due to the elastic strain that arose in the sample (Fig. 2b). However, the diffraction pattern was still $P2_1/c$. With increasing temperature along path 1, the diffraction peaks become sharp by the relaxation of the elastic strain in the sample. When the sample was heated to 873 K (c) on path 1, the diffraction pattern of $C2/c$ appeared along with $P2_1/c$ (Fig. 2c). After quenching the sample to room temperature (d), the $P2_1/c$ and $C2/c$ peaks were both observed (Fig. 2d). During the compression to 10.7 GPa (e), $C2/c$ peaks gradually became stronger and $P2_1/c$ peaks became weaker. In this process, the broadening of the diffraction peaks was inconspicuous (Fig. 2e). When temperature was raised to 873 K (f) along path 2, $P2_1/c$ peaks disappeared and only $C2/c$ peaks were observed (Fig. 2f). After this, in the whole course of path 3 and up to point (k) on path 4, the diffraction patterns showed only the $C2/c$ phase (Figs. 2g–2k). When temperature was raised to 1473 K (l), however, $C2/c$ peaks disappeared and orthoenstatite peaks with space group *Pbca* appeared (Fig. 2l). The phases detected are also shown by the symbols on the *P-T* paths in Figure 1.

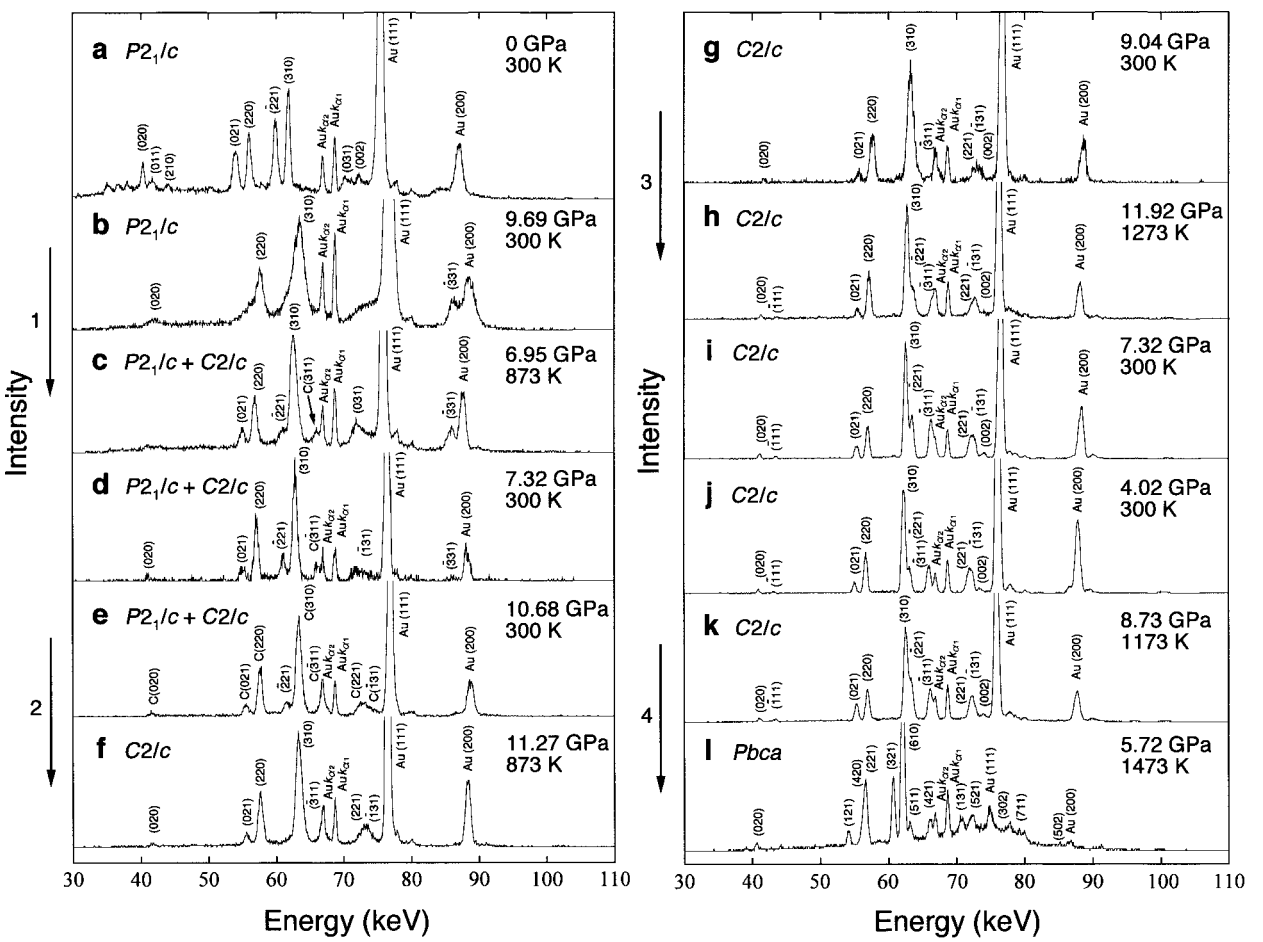

FIGURE 2. Energy-dispersive X-ray diffraction patterns of enstatite at the indicated pressure and temperature taken at the points a–l in Figure 1. The arrows numbered 1 to 4 on the left sides of the patterns correspond to the *P-T* paths 1 to 4 in Figure 1. Reduction of the ($\bar{2}$21) reflection of $P2_1/c$ and splitting of the (310) reflection into two observed in **c**–**i**, show the transition from the $P2_1/c$ to high-*P* $C2/c$ phase. A typical pattern of the high-*P* $C2/c$ phase is shown in **i**. The reflections indexed for $C2/c$ are marked with C in **c**, **d**, and **e**.

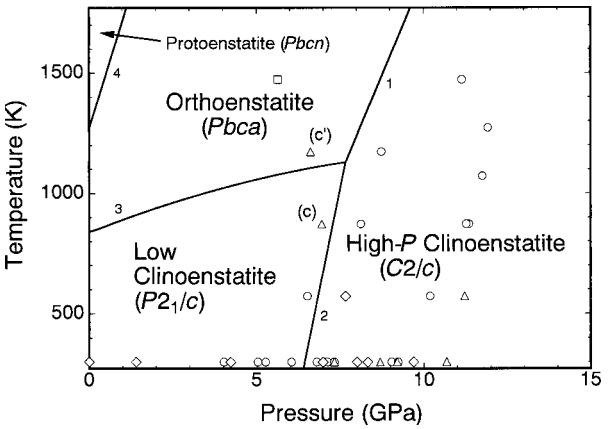

FIGURE 3. Observed phases by the in situ X-ray diffraction experiments superimposed on the phase diagram of enstatite. For symbols, see Figure 1. The orthoenstatite–high-*P* clinoenstatite boundary 1 is determined from the quenching method using a MAC by Pacalo and Gasparik (1990), while the orthoenstatite–protoenstatite boundary 4 is from Chen and Presnall (1975). The boundaries 2 and 3 are calculated by Angel and Hugh-Jones (1994), using the room-temperature equations of state for orthoenstatite, low clinoenstatite, and high-*P* clinoenstatite combined with the d*P*/d*T* slopes of the orthoenstatite–high-*P* clinoenstatite boundary by Pacalo and Gasparik (1990) and the orthoenstatite–low clinoenstatite boundary by Grover (1972).

TABLE 1. Unit-cell parameters of enstatite at various pressure and temperature conditions

P (GPa)	*T* (K)	*a* (Å)	*b* (Å)	*c* (Å)	β (°)	*V* (Å³)
			P*2₁/*c			
0.00	300	9.599(3)	8.816(2)	5.170(1)	108.16(3)	415.8(2)
1.40	300	9.520(5)	8.776(3)	5.147(2)	107.81(5)	409.5(3)
4.22	300	9.413(2)	8.750(2)	5.111(1)	107.65(2)	401.2(1)
6.98	300	9.388(3)	8.695(2)	5.046(1)	107.61(3)	392.6(2)
8.00	300	9.370(3)	8.651(2)	5.036(1)	107.34(3)	389.7(2)
8.32	300	9.357(4)	8.648(3)	5.035(2)	107.31(5)	389.0(3)
9.69	300	9.342(6)	8.613(5)	5.014(3)	107.27(7)	385.2(4)
7.66	573	9.390(4)	8.703(3)	5.057(2)	107.65(4)	393.8(2)
6.95	873	9.420(3)	8.722(2)	5.096(1)	107.72(3)	398.8(2)
6.61	1173	9.479(5)	8.750(4)	5.134(3)	107.83(5)	405.4(3)
7.32	300	9.378(7)	8.672(5)	5.042(4)	107.50(8)	391.1(4)
8.69	300	9.345(4)	8.636(3)	5.033(2)	107.30(5)	387.8(3)
9.20	300	9.353(6)	8.629(5)	5.024(3)	107.29(7)	387.1(4)
10.68	300	9.305(2)	8.593(1)	5.0106(9)	107.25(2)	382.6(1)
			C*2/*c			
6.61	1173	9.289(3)	8.713(2)	4.952(2)	101.69(3)	392.4(2)
7.32	300	9.225(5)	8.610(2)	4.907(2)	101.51(5)	381.9(2)
8.69	300	9.160(8)	8.603(3)	4.901(2)	101.50(6)	378.5(4)
9.20	300	9.128(5)	8.598(3)	4.902(3)	101.46(10)	377.0(3)
10.68	300	9.095(8)	8.578(4)	4.887(4)	101.41(5)	373.8(4)
11.22	573	9.102(7)	8.567(4)	4.896(4)	101.44(14)	374.2(4)
11.27	873	9.119(5)	8.594(2)	4.899(3)	101.49(9)	376.3(3)
9.23	300	9.125(5)	8.597(3)	4.901(3)	101.43(9)	376.9(3)
9.04	300	9.133(7)	8.603(3)	4.905(4)	101.47(13)	377.6(4)
10.19	573	9.117(7)	8.596(3)	4.900(3)	101.44(10)	376.4(3)
11.35	873	9.118(4)	8.592(2)	4.899(2)	101.48(8)	376.1(3)
11.75	1073	9.124(3)	8.589(2)	4.900(1)	101.54(3)	376.2(2)
11.92	1273	9.184(3)	8.593(2)	4.892(1)	101.61(2)	378.2(2)
11.14	1473	9.224(3)	8.626(2)	4.912(2)	101.62(3)	382.8(2)
7.11	300	9.207(3)	8.620(4)	4.915(2)	101.52(4)	382.2(3)
7.01	300	9.219(1)	8.624(1)	4.9139(8)	101.52(2)	382.8(1)
6.80	300	9.235(3)	8.638(2)	4.911(2)	101.54(3)	383.9(2)
6.04	300	9.238(2)	8.658(2)	4.920(1)	101.55(2)	385.5(1)
5.26	300	9.250(5)	8.668(4)	4.933(2)	101.59(5)	387.4(3)
4.02	300	9.277(4)	8.709(5)	4.943(3)	101.60(5)	391.2(4)
5.03	300	9.249(6)	8.682(5)	4.940(3)	101.59(7)	388.6(4)
6.52	573	9.247(3)	8.666(3)	4.922(2)	101.61(3)	386.3(2)
8.12	873	9.233(3)	8.640(2)	4.920(2)	101.59(3)	384.5(2)
8.73	1173	9.239(2)	8.663(2)	4.917(1)	101.64(2)	385.5(2)
			Pbca			
5.72	1473	18.179(1)	8.768(2)	5.1432(9)	90.0	819.8(2)

Note: Estimated uncertainties in pressure and temperature are less than 50 K and 0.4 GPa, respectively.

The phases observed here are superimposed on the phase diagram of enstatite previously reported (Fig. 3). Our in situ X-ray diffraction experiments confirm that the monoclinic *C*2/*c* phase has a wide stability field on the high pressure side of orthoenstatite and low clinoenstatite. Although most of the observed phases are consistent with Figure 3, a large pressure hysteresis of the $P2_1/c$–*C*2/*c* transition at room temperature was observed. At room temperature compression, low clinoenstatite was observed up to 10.7 GPa, and high-*P* *C*2/*c* clinoenstatite did not revert to the $P2_1/c$ phase even at 4.0 GPa on pressure release. This pressure hysteresis is larger than that observed by Angel et al. (1992) using a DAC. This difference in pressure hysteresis between both groups may be due to the fact that non-hydrostatic stresses arose in a MAC or the run durations used here are not long enough for the transition to occur. Also in Figure 3, some points such as (c) and (c') are not consistent with this phase diagram of enstatite. However, the time durations and/or temperatures of the present in situ X-ray experiments at those points will not be sufficient for the phase transitions, and the direct application of the present data to the analyses of equilibrium relationships of the phase diagram will not be adequate.

Refined unit-cell parameters at the indicated points on the *P*-*T* paths are given in Table 1. The unit-cell parameters of the high-*P* *C*2/*c* phase at 7.32 GPa and room temperature in this study are in good agreement with those of high pressure in situ single crystal X-ray diffraction study using a DAC at 7.93 GPa and room temperature by Angel et al. (1992). The unit-cell volume of the high-*P* *C*2/*c* phase is constantly about 10 Å³ (2.5%) smaller in the unit-cell volume than the $P2_1/c$ phase at pressures between 4.0 GPa and 10.7 GPa at room temperature, and the differences seem to increase with temperature (Fig. 4).

The β angle of the $P2_1/c$ phase varies from 107.3° to 108.2° with pressure (Fig. 5), showing very little variation with temperature and pressure, whereas the β angle of the *C*2/*c* phase varies from 101.4° to 101.7°, also showing little variation with temperature and pressure. The latter values of the *C*2/*c* phase are about 8° smaller than that of the high-*T* *C*2/*c* phase reported by Smith (1969), and also about 4° smaller than that of diopside (Clark et al. 1969) that has a *C*2/*c* structure at ambient conditions. Hugh-Jones et al. (1994) performed the room-temperature single crystal compression study using a DAC and suggested that the structure of the high-*P* *C*2/*c* phases are significantly different from those of the high-*T* *C*2/*c* phases and *C*2/*c* pyroxenes containing Ca. Our in situ high pressure and high temperature data confirmed their suggestion.

TABLE 2. Equations of state parameters of low clinoenstatite and high-*P* clinoenstatite

V_0 (Å^3)	K_0 (GPa)	K_0'	$(\partial K_T/\partial T)_P$ (GPa/K)	$\alpha(T) = a_0 + a_1 T$ $a_0(10^{-5}\,K^{-1})$	$a_1(10^{-8}\,K^{-2})$	Reference
			P2$_1$/c			
415.4 (5)	108.5 (6.4)	4.5 (1.3)	–	–	–	This study
414.6 (1)	111.1 (3.3)	6.6 (1.1)	–	–	–	Angel and Hugh-Jones (1994)
			C2/c			
405.1 (1.7)	106.4 (17.4)	5.4 (2.7)	–	–	–	This study
405.0 (2.6)	106.9 (25.9)	5.3 (3.0)	–0.021 (10)	2.01 (44)	2.10 (1.1)	This study
405.6 (1.1)	104.1 (5.7)	6.6*	–	–	–	Angel and Hughes-Jones (1994)

* This value was fixed during the least squares refinements.

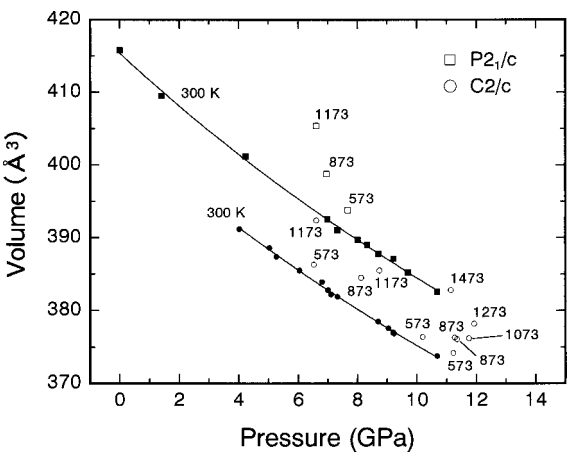

FIGURE 4. Variations of the unit-cell volumes of $P2_1/c$ low clinoenstatite and high-*P* $C2/c$ clinoenstatite with pressure. Solid symbols correspond to the room-temperature data, while open symbols represent the high-temperature data. Error bars in volume are smaller than the symbol size. The labels next to the data points are the temperatures in K. Squares represent the data of the $P2_1/c$ phase and circles are the high-*P* $C2/c$ phase. The solid curves represent the best fits of the room-temperature data using a third-order Birch-Murnahan equation of state.

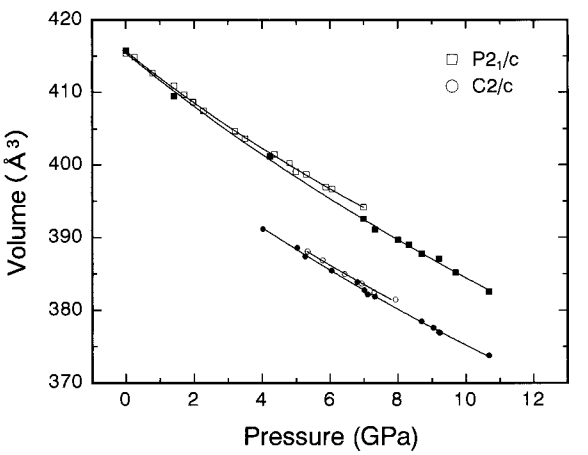

FIGURE 6. Comparison of the pressure-volume data of $P2_1/c$ low clinoenstatite (squares) and high-*P* $C2/c$ clinoenstatite (circles) at room-temperature between the present study and the previous single crystal experiment using a DAC (Angel and Hugh-Jones 1994). Solid symbols correspond to the data of this study and open symbols are from Angel and Hugh-Jones (1994). The solid curves represent the equations of state for the $P2_1/c$ and high-*P* $C2/c$ phases.

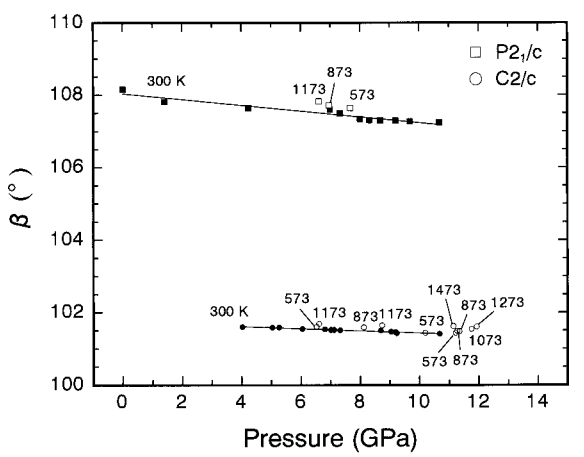

FIGURE 5. Variations of β in $P2_1/c$ low clinoenstatite (squares) and high-*P* $C2/c$ clinoenstatite (circles) with pressure. Error bars in β are smaller than the symbol size. Solid symbols correspond to the room-temperature data, open symbols show the high-temperature data. The labels next to the data points are the temperatures in K. Solid lines are the linear fits of the room-temperature data.

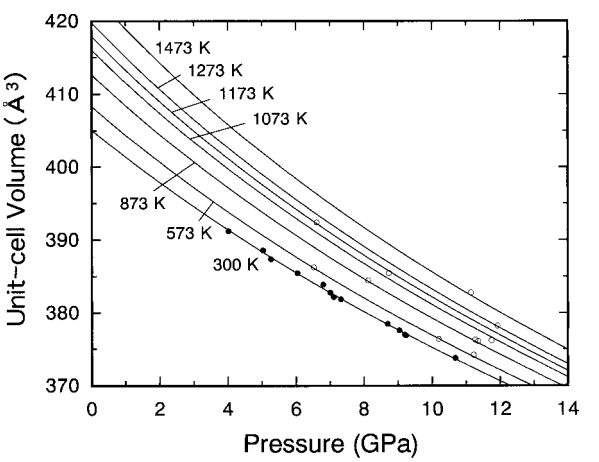

FIGURE 7. Calculated isothermal compression curves of high-*P* $C2/c$ clinoenstatite between 300 and 1473 K using the determined HTBM equation of state. Solid circles denote the data obtained at room temperature and open circles are the data obtained at high temperatures.

Equations of state

Table 2 lists the parameters of the room-temperature equations of state derived by least-squares fitting of the room-temperature data of high-*P* *C*2/*c* and $P2_1/c$ clinoenstatite (Table 1) to Equation 2. The fitted isothermal curves are shown in Figure 6, along with the previous results of Angel and Hugh-Jones (1994) for comparison. The K_0 values determined here are nearly the same as those of Angel and Hugh-Jones (1994) for both the *C*2/*c* and $P2_1/c$ phases. Although the K_0' values for both the $P2_1/c$ and high-*P* *C*2/*c* phases are consistent with those of Angel and Hugh-Jones (1994) within estimated standard deviations, these are slightly smaller (4.5 for the $P2_1/c$ phase and 5.4 for the *C*2/*c* phase) than their values (6.6 for both the $P2_1/c$ and *C*2/*c* phases), as also seen in Figure 6. Non-hydrostatic stress may significantly affect both the determinations of pressure and the unit-cell parameters (Weidner et al. 1992; 1994; Martinez et al. 1996; Zhang et al. 1997). However, we do not think that somewhat smaller K_0' values come from differential stress that might have arisen, because the volumes determined from some of the diffraction profiles that suffered non-hydrostatic stress, do not show any significant deviation from those of other data for which this stress had already relaxed. Also, the K_0' value determined in the high-temperature equation of state described in the next paragraph, is consistent with that of the room-temperature equation of state.

For the *C*2/*c* phase, we fit all the pressure-volume-temperature data to a HTBM equation of state. The final refined values of V_0, K_0 and K_0' from this calculation (Table 2) were almost the same as the parameters of the room-temperature equation of state. In the calculation of $\alpha(T)$, the T^{-2} term was neglected because when $\alpha(T)$ was expressed as:

$$\alpha(T) = a_0 + a_1 T - a_2 T^{-2}, \quad (6)$$

where a_2 converged to the negative value in the least-squares fitting.

Although some thermal expansion coefficients of $P2_1/c$ clinoenstatite and orthoenstatite have been reported, no previous data exist for that of the high-*P* *C*2/*c* phase. Hugh-Jones (1997) reported the mean volume thermal expansion coefficients of 2.99 (11) $\times 10^{-5}$ K^{-1} for $P2_1/c$ clinoenstatite and 3.22 (11) $\times 10^{-5}$ K^{-1} for orthoenstatite. Our volume thermal expansion coefficient of the high-*P* *C*2/*c* phase is temperature dependent and its value at low temperature is smaller than those of Hugh-Jones (1997), while the value at high temperature is larger than those.

The isothermal compression curves of the high-*P* *C*2/*c* phase calculated from the obtained equation of state at high pressure and high temperature (Table 2) are shown in Figure 7 along with the observed data used for the fitting. The observed unit-cell volumes at pressures up to 12 GPa and temperatures up to 1473 K are well reproduced by the determined equation of state.

In conclusion the present high pressure and high temperature in situ X-ray diffraction experiments up to 12 GPa and 1473 K confirm the phase transitions and physical properties of $MgSiO_3$ enstatite. The structure of the high-*P* *C*2/*c* phase is characterized by small β angles of 101.4° to 101.7°, with almost no dependence on temperature and pressure. The high-*P* *C*2/*c* phase is thus structurally quite distinct from the high-*T* *C*2/*c* phase even at high temperature, as suggested by Hugh-Jones et al. (1994). The unit-cell volumes of the high-*P* *C*2/*c* phase are about 10 Å^3 (2.5%) smaller than those of the $P2_1/c$ phase at same pressures and room temperature, and the difference between both phases seems to increase with temperature.

ACKNOWLEDGMENTS

The authors are grateful to M. Miyashita, N. Kubo, M. Isshiki, Y. Yamasaki, N. Nishiyama, and T. Uchida for their helpful support for in situ X-ray diffraction experiments, and T. Katsura for his computer programming techniques for refinement of the equation of state parameters. We also thank N. Funamori, T. Kubo, D. Kaushik, and N. Miyajima for useful discussions and R. Sorkhabi for reviewing the manuscript. The experiments were performed at the National Laboratory for High Energy Physics (K.E.K.). This work was supported by the Grant-in-Aid for Research (no. 06402019) from the Ministry of Education, Science and Culture of the Japanese Government.

REFERENCES CITED

Atlas, L. (1952) The polymorphism of $MgSiO_3$ and solid-state equilibria in the system $MgSiO_3$-$CaMgSi_2O_6$. Journal of Geology, 60, 125–147.

Anderson, O.L., Isaak, D.G., and Yamamoto, S. (1989) Anharmonicity and the equation of state for gold. Journal of Applied Physics, 65, 1534–1543.

Angel, R.J. and Hugh-Jones, D.A. (1994) Equations of state and thermodynamic properties of enstatite pyroxenes. Journal of Geophysical Research, 99, 19777–19783.

Angel, R.J., Chopelas, A., and Ross, N.L. (1992) Stability of high-density clinoenstatite at upper-mantle pressures. Nature, 358, 322–324.

Boyd, F.R. and England, J.L. (1965) The rhombic enstatite-clinoenstatite inversion. Carnegie Institution of Washington Year Book, 64, 117-120.

Boyd, F.R. and Schairer, J.F. (1964) The system $MgSiO_3$-$CaMgSi_2O_6$. Journal of Petrology, 5, 275–309.

Brown, W.L. and Smith, J.V. (1963) High-temperature X-ray studies on the polymorphism of $MgSiO_3$. Zeitschrift für Kristallographie, 118, 186–212.

Chen, C.-H. and Presnall, D.C. (1975) The system Mg_2SiO_4-SiO_2 at pressures up to 25 kilobars. American Mineralogist, 60, 398–406.

Chopelas, A. and Boehler, R. (1992) Raman spectroscopy of high pressure $MgSiO_3$ phases synthesized in a CO_2 laser heated diamond anvil cell: Perovskite and clinopyroxene. In Y. Syono and M.H. Manghnani, Eds., High pressure research: Application to earth and planetary sciences, p. 101–108. Terra Scientific Publishing Company, Tokyo/American Geophysical Union, Washington, D.C.

Clark, J.R., Appleman, D.E., and Papike, J.J. (1969) Crystal-chemical characterization of clinopyroxenes based on eight new structure refinements. Mineralogical Society of American Special Paper, 2, 31–50.

Coe, R.S. (1970) The thermodynamic effect of shear stress on the ortho-clino inversion in enstatite and other coherent phase transitions characterized by a finite simple shear. Contributions to Mineralogy and Petrology, 26, 247–264.

Gasparik, T. (1990) A thermodynamic model for the enstatite-diopside join. American Mineralogist, 75, 1080–1091.

Grover, J. (1972) The stability of low-clinoenstatite in the system $Mg_2Si_2O_6$-$CaMgSi_2O_6$ (abstract). EOS, Transactions, American Geophysical Union, 53, 539.

Hugh-Jones, D.A., Woodland, A.B., and Angel, R.J. (1994) The structure of high-pressure *C*2/*c* ferrosilite and crystal chemistry of high-pressure *C*2/*c* pyroxenes. American Mineralogist, 79, 1032–1041.

Hugh-Jones, D. (1997) Thermal expansion of $MgSiO_3$ and $FeSiO_3$ ortho- and clinopyroxenes. American Mineralogist, 82, 689–696.

Iishi, K. and Kitayama, H. (1995) Stability of high clinoenstatite. Neues Jahrbuch für Mineralogie Monatshefte, 2, 65–74.

Irifune, T., Utsumi, W., and Yagi, T. (1992) Use of a new diamond composite for multianvil high-pressure apparatus. Proceedings of the Japan Academy, 68, 161–166.

Irifune, T. et al. (1998) X-ray diffraction measurements in a double-stage multianvil apparatus using ADC anvils. In M.H. Manghnani and T. Yagi, Eds., Properties of earth and planetary materials at high pressure and temperature, p. 1–8. American Geophysical Union, Washington, D.C.

Kanzaki, M. (1991) Ortho/Clinoenstatite transition. Physics and Chemistry of Minerals, 17, 726–730.

Martinez, I., Zhang, J., and Reeder, R.J. (1996) In situ X-ray diffraction of aragonite and dolomite at high pressure and high temperature. American Mineralogist, 81, 611–624.

Morimoto, N. and Koto, K. (1969) The crystal structure of orthoenstatite. Zeitschrift für Kristallographie, 129, 65–83.

Morimoto, N., Appleman, D.E., and Evans, H.T. Jr. (1960) The crystal structures of clinoenstatite and pigeonite. Zeitschrift für Kristallographie, 114, 120–147.

Munoz, J.L. (1968) Effect of shearing on enstatite polymorphism. Carnegie Institution of Washington Year Book, 66, 369–370.

Pacalo, R.E.G. and Gasparik, T. (1990) Reversals of the orthoenstatite-clinoenstatite transition at high pressures and high temperatures. Journal of Geophysical Research, 95, 15853–15858.

Raleigh, C.B. and Kirby, S.H. (1971) Slip and the clinoenstatite transformation as competing rate processes in enstatite. Journal of Geophysical Research, 76, 4011-4022.

Riecker, R.E. and Rooney, T.P. (1967) Deformation and polymorphism of enstatite under shear stress. Geological Society of America Bulletin, 78, 1045–1054.

Saxena, S.K. and Zhang, J. (1990) Thermochemical and pressure-volume- temperature systematics of data on solids, examples; Tungsten and MgO. Physics and Chemistry of Minerals, 17, 45–51.

Sadanaga, R. and Okamura, F. (1971) On the high-clino phase of enstatite. Mineralogical Journal, 6, 365–374.

Sclar, C.B., Carrison, L.C., and Schwartz, C.M. (1964) High pressure stability fields of clinoenstatite, and the orthoenstatite-clinoenstatite transition (abstract). EOS, Transactions, American Geophysical Union, 45, 121.

Shimobayashi, N. and Kitamura, M. (1991) Phase transition in Ca-poor clinopyroxenes. Physics and Chemistry of Minerals, 18, 153–160.

——(1993) Phase transition of orthoenstatite to high-clinoenstatite: in situ TEM study at high temperature. Mineralogical Journal, 16, 416–426.

Shimomura, O., Yamaoka, S., Yagi, T., Wakatsuki, M., Tsuji, K., Kawamura, H., Hamaya, N., Fukunaga, O., Aoki, K., and Akimoto, S. (1985) Multi-anvil type X-ray system for synchrotron radiation. In S. Minomura, Ed., Solid state physics under pressure: Recent Advances with Anvil Devices, p. 351–356. KTK Scientific Publishers, Tokyo/Reidel, Dordrecht.

Smith, J.V. (1969) Magnesium pyroxenes at high temperature: Inversion in clinoenstatite. Nature, 222, 256–257.

Smyth, J.R. (1971) Protoenstatite: a crystal-structure refinement at 1100 °C. Zeitschrift für Kristallographie, 134, 262–274.

——(1974) Experimental study on the polymorphism of enstatite. American Mineralogist, 59, 345-352. Physics and Chemistry of Minerals, 22, 300–310.

Weidner, D.J., Vaughan, M.T., Ko, J., Wang, Y., Liu, X., Yeganeh-Haeri, A., Pacalo, R.E., and Zhao, Y. (1992) Characterization of stress, pressure and temperature in SAM 85, a DIA type high pressure apparatus. In Y. Syono and M.H. Manghnani, Eds., High pressure research: Application to earth and planetary sciences, p. 13–17. Terra Scientific Publishing Company, Tokyo/American Geophysical Union, Washington, D.C.

Weidner, D.J., Wang, Y., and Vaughan, M.T. (1994) Yield strength at high pressure and temperature. Geophysical Research Letters, 21, 753–756.

Yang, H. and Ghose, S. (1995) High temperature single crystal X-ray diffraction studies of the ortho-proto phase transition in enstatite, $Mg_2Si_2O_6$ at 1360 K. Physics and Chemistry of Minerals, 22, 300–310.

Yamamoto, K. and Akimoto, S. (1977) The system MgO-SiO_2-H_2O at stability field for hydroxyl-chondrodite, hydroxyl-clinohumite and 10 phase. American Journal of Science, 277, 288–312.

Yagi, T. (1988) MAX80: Large-volume high-pressure apparatus combined with synchrotron radiation. EOS, Transactions, American Geophysical Union, 69, 18–27.

Zhang, J., Martinez, I., Guyot, F., Gillet, P., and Saxena, S.K. (1997) X-ray diffraction study of magnesite at high pressure and high temperature. Physics and Chemistry of Minerals, 24, 122–130.

MANUSCRIPT RECEIVED AUGUST 10, 1998
MANUSCRIPT ACCEPTED JUNE 11, 1999
PAPER HANDLED BY WILLIAM A. BASSETT